Modeling Wide Bandgap GaInP Photovoltaic Cells For Conversion Efficiencies Up to 16.5%

Yubo Sun[1], Kyle H. Montgomery[2], Xufeng Wang[1], Stephanie Tomasulo[4], Minjoo Larry Lee[3], Peter Bermel[1]

[1]Purdue University, West Lafayette, IN, 47907, U.S.A.

[2]University of California, Davis, CA, 95616, U.S.A.

[3]Yale University, New Haven, CT, 06520, U.S.A.

[4]U.S. Naval Research Lab, Washington, DC, 20375, U.S.A.

***Abstract* — Here we consider how to accurately model and design wide bandgap (E_g = 2.1 eV) GaInP photovoltaic cells. Detailed absorption data for the Ga-rich alloy is obtained by extrapolating literature values for InP and $Ga_{0.5}In_{0.5}P$. We then combined these values with estimates of carrier lifetime (0.1 ns) and interface recombination ($9x10^5$ cm/s) to construct detailed electro-optical models. They are found to accurately reproduce the EQE, J_{sc}, and V_{oc} observed in published experimental devices. Small discrepancies of 0.1% are caused by slight differences in optical constants and interface recombination. This modeling process illustrates the major sources of loss, namely interface recombination between the emitter and window layer and low bulk minority carrier lifetimes in the active region. An improved design is also proposed, which involves adjusting the doping and thickness of key layers. These findings will help define a path towards increasing the performance of these wide bandgap cells to approach their theoretical limit – approximately 16.5%.**

***Index Terms* — InGaP, modeling, molecular beam epitaxy, n-i-p, wide-bandgap.**

I. Introduction

For the past decades, photovoltaic systems have been designed and fabricated to reach ultra-high efficiencies well above the single-junction Shockley-Queisser limit [1], requiring wide bandgap solar cells. For example, if multiple PV cells are stacked together in series, a wide bandgap cell (> 2.0 eV) is needed to achieve the most efficient conversion of high energy photons [2]. Similarly, spectral splitting requires a wide bandgap cell for maximally effective conversion [3]. Photovoltaics at elevated temperatures also suffer from less degradation with a wide bandgap cell [4]-[5]. Finally, for near-surface underwater PV applications of recent interest, there is a need for wide bandgap cells for efficient collection of the high energy photons that can penetrate water [6].

In this manuscript, we consider a wide bandgap GaInP photovoltaic cell (E_g=2.1 eV at 27°C) deposited on a transparent GaP substrate (E_g =2.26 eV at 27°C). The transparent GaP substrate, like many III-V substrates, allows photons with energy below the bandgap of the active junction to be highly transmitted. Solar cells located behind GaAs substrates have shown internal quantum efficiencies (IQE) in the infrared approaching 90% [7], and the low absorption loss of GaP below its bulk bandgap is well-known from its use in transparent-substrate visible light-emitting diodes [8].

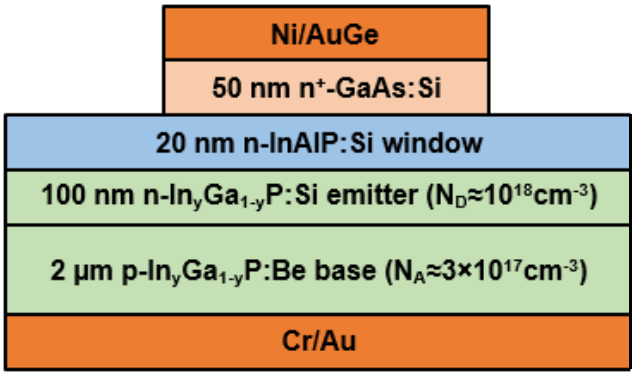

Fig. 1. Cross-sectional schematic of $Ga_{1-y}In_yP$ cell structure modeled in this work (adapted from [12]).

The current state-of-the-art solution for accessing the 2.1-2.2 eV E_g range, while retaining a direct bandgap, is to increase the Al content in quaternary $(Al_xGa_{1-x})_{0.51}In_{0.49}P$, grown lattice-matched to GaAs [9]. However, it has been found that the oxygen incorporation associated with increased Al content decreases solar cell efficiency [10]. Further, a GaAs substrate is not transparent to light below the bandgap of the active junction. Another wide bandgap option is GaP, with an indirect bandgap of 2.26 eV. GaP should be a natural choice, considering the availability of high-quality bulk substrates and the commercial maturity of GaP-based light emitting diodes. However, GaP solar cells suffer from relatively poor absorption and current collection, with IQE values typically peaking at ~50% [17,18]; as a result, the highest efficiency for anti- reflection (AR)-coated cells in the literature is 2.9% [11].

As an alternative, direct bandgap $Ga_{1-y}In_yP$ ($0.18 < y < 0.30$) solar cells can be grown by molecular beam epitaxy (MBE) using metamorphic (MM) buffers on GaAs or GaP substrates. The direct bandgap enables stronger absorption and higher short-circuit current density, J_{sc}, than has been conventionally possible in GaP solar cells. However, the challenge in growing $Ga_{1-y}In_yP$ ($0.18 < y < 0.30$) cells is that they are lattice-mismatched to conventional substrates, as illustrated in Fig. 2.

The red dot highlights the bandgap energy and lattice constant of $Ga_{0.75}In_{0.25}P$ modeled in this work. To grow lattice-mismatched $Ga_{1-y}In_yP$ films with low threading dislocation

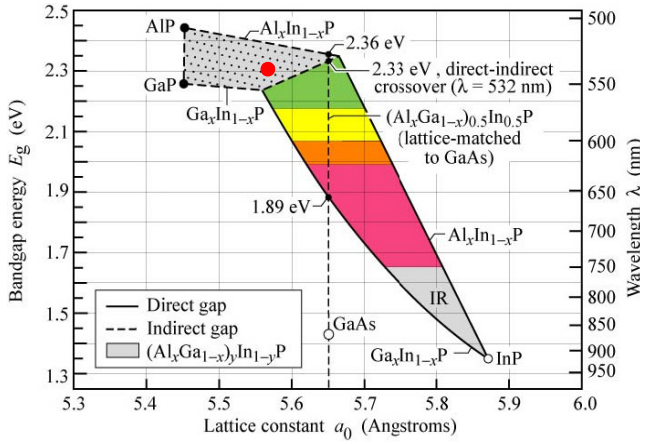

Fig. 2. Bandgap energy and corresponding wavelength versus lattice constant of $(Al_xGa_{1-x})_yIn_{1-y}P$ at 300K (adapted from [15]). Our study focuses on $Ga_{0.75}In_{0.25}P$ (E_g=2.19 eV) (red dot)

densities (TDDs) and long minority carrier lifetimes, intermediate $GaAs_xP_{1-x}$ graded buffers can be used to engineer the lattice constant from that of the GaP substrate to that of the wide bandgap $Ga_{1-y}In_yP$ solar cell. Prior work on these devices has shown an open circuit voltage, V_{oc}, of 1.42 V, J_{sc} of 3.11 mA/cm^2 (without anti-reflection coating), and a fill factor (FF) of 0.71, yielding a cell efficiency of 3.13% [12].

II. Modeling Approach

Modeling the performance of such a cell design first requires an accurate model of material absorption. Since no literature data is currently available, this can be extrapolated from related III-V compounds. Fig. 2 also illustrates the bandgap energy transition from InP to GaP, where the black solid line shows direct bandgap transitions, and the black dashed line describes the indirect bandgap transition. The absorption data of $Ga_{0.5}In_{0.5}P$ and InP were used to extrapolate the absorption data of $Ga_{0.75}In_{0.25}P$. In order to achieve this, the band edges of the three materials mentioned above were identified. The extrapolation method employed was to horizontally shift the absorption curves of $Ga_{0.5}In_{0.5}P$ and InP towards shorter wavelengths, based on the band edge ratios. The extrapolated absorption curve of $In_{0.25}Ga_{0.75}P$ is shown in Fig. 3: its implied band edge wavelength is 566 nm, which directly matches its bandgap energy of 2.19 eV. This should be a reliable way to generate the absorption data of $Ga_{0.75}In_{0.25}P$, as all materials being considered in this extrapolation are direct bandgap materials.

The simulation tool used to model the wide-E_g GaInP cell is "A Device Emulation Program and Tool" (ADEPT), available

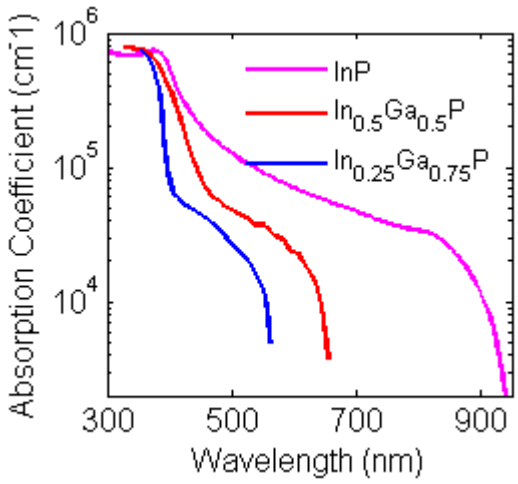

Fig. 3. Extrapolated absorption curve of $In_{0.25}Ga_{0.75}P$, calculated from literature data for the absorption of InP and $In_{0.5}Ga_{0.5}P$.

on nanoHUB.org [14]. This tool solves Poisson's equation with hole and electron continuity equations in 1 spatial dimension in compositionally non-uniform semiconductors. It was originally written to model solar cells fabricated from a wide variety of materials including a-Si, CIGS, CdTe, etc. [14]

III. Results and Discussion

The external quantum efficiency (EQE) was calculated for a cell structure consisting of a 20 nm window layer of n-AlInP, 100 nm emitter of n-$Ga_{0.75}In_{0.25}P$ (N_D=10^{18}/cm^3), and 2 µm of p-$Ga_{0.75}In_{0.25}P$ (N_A=3x10^{17}/cm^3), as shown in Fig. 1. Due to the fact that the window layer of this cell is made of AlInP, a

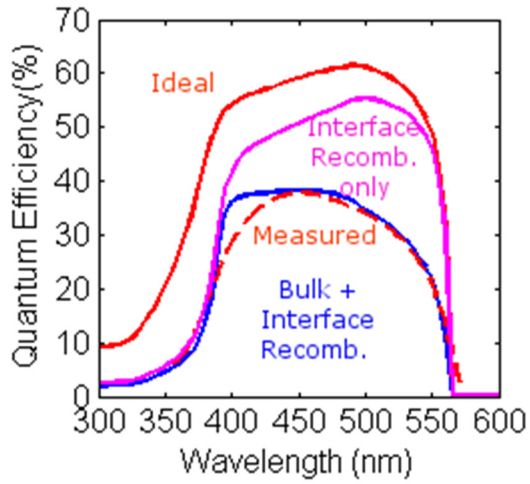

Fig. 4. External quantum efficiency (EQE) versus wavelength from 300 nm to 600 nm. Experimental data (dashed red line) is from Ref. 12. The model fit accounts for ideal (red), interface recombination only (green) and both interface and bulk recombination effects (blue).

heterostructure was formed at the interface between the window layer and the GaInP emitter, and the density of defects is not negligible at the interface. Thus, interface recombination also contributes to the degradation of the cell performance. The simulated EQE for various levels of recombination compared to the experimental EQE is shown in Fig. 4. The ideal case with high bulk lifetime (1 ms) and low window-emitter recombination (< 1 cm/s) predicts exceedingly high EQE values. Degrading just one of these values alone is also insufficient to account for the observed EQE. Instead, it was found that both the emitter and base minority carrier lifetime (τ_e and τ_b) must be reduced to 0.12ns and 0.1 ns respectively, which shows some agreement to the bulk minority carrier lifetime characterized and reported in the literature [16]. At the same time, the window-emitter interface recombination velocity must increase to $9\text{x}10^5$ cm/s to match the measured EQE curve (from [12]). This allows the J_{sc} from the simulation to agree closely with the J_{sc} reported in the experiment.

In order to fully capture the I-V characteristics of the cell, J_{sc} and V_{oc} were calculated as follows. First, equation (1) was used to characterize the shape of the simulated I-V curve:

$$J_{sc} = \int_0^\infty d\lambda \left[\frac{e\lambda}{hc}\frac{dI}{d\lambda}\text{EQE}(\lambda)\right] \quad (1)$$

Here, J_{sc} is given as the product of the AM 1.5G solar spectrum and the EQE integrated over all wavelengths. The calculated J_{sc} is 3.16 mA/cm^2, which is slightly higher than the measured J_{sc}. This difference can be attributed to small deviations between simulated and measured EQE around 400 nm shown in Fig. 4. The disagreement of EQE at this wavelength range is mainly due to imperfections in the wide E_g material absorption modeling, which could be improved by considering a piecewise mathematical model of the dispersion of the imaginary part of refractive index presented in literature [13].

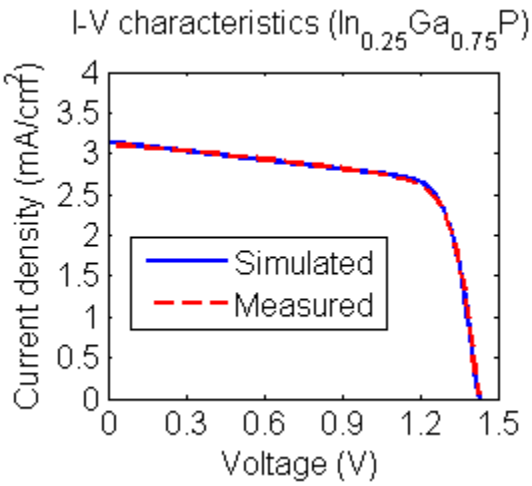

Fig. 5. A comparison between measured and simulated I-V characteristics of the single junction $Ga_{0.75}In_{0.25}P$ solar cell. Very strong agreement in V_{oc} and fill factor and J_{sc} is observed, derived from the EQE in Fig. 3.

The open circuit voltage is obtained directly from ADEPT. The diode equation used to model the experimental data, which incorporates ideality factor, series and shunt resistance is given as Equation (2):

$$J(V) = J_{sc} - J_o \exp\left[\frac{e(V + JR_s) - E_g}{nkT}\right] - \frac{V + JR_s}{R_{sh}} \quad (2)$$

The calculated ideality factor is 1.61. Finally, reasonable values of the series and shunt resistance (20 mΩ-cm^2 and 2.7 kΩ-cm^2, respectively) were added to achieve the closest possible fit to experiment, as shown in Fig. 5. An excellent match was achieved, with an average difference between the two curves of 0.1%.

IV. Improvement of Cell Structure

After reproducing the measured data successfully, we consider strategies to optimize cell efficiency. Based on the extrapolated absorption curve of wide-E_g GaInP in Fig. 3, it can be concluded that most photons are absorbed near the front surface. Thus, the carrier collection efficiency at the contact is very sensitive to the doping level and thickness of the emitter layer. Theoretically, low doping in the emitter leads to high minority carrier lifetimes and long diffusion lengths, which could increase the possibility of carriers reaching at the contact before recombining. However, it could also hurt the built-in potential at the junction to reduce the V_{oc}, offsetting the improvement in J_{sc}. Therefore, it is worth exploring this tradeoff to help maximize the cell efficiency. There is also a similar tradeoff in terms of emitter thickness, as it determines the location of the depletion region where a strong electric field

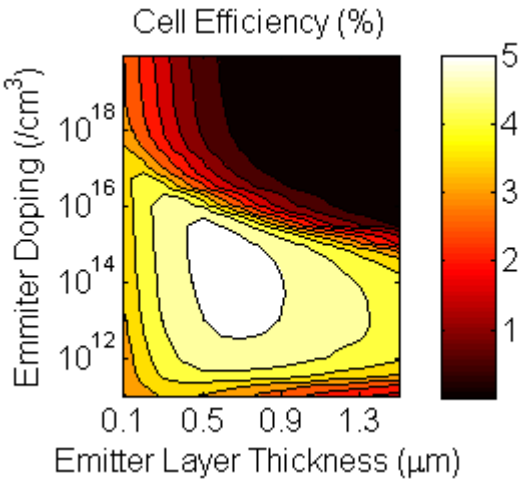

Fig. 6. A contour plot optimizing the cell efficiency as a function of emitter layer parameters, specifically doping and thickness.

is formed to help dissociate electron-hole pairs and sweep electrons and holes towards the metallic contact. Carrier

collection is more efficient as the emitter thins out to keep the space charge region close to the surface of the cell where the majority of electron-hole pairs are generated. However, it is difficult to fabricate ultra-thin heavily doped layers with typical fabrication techniques. The correlation of cell efficiency with emitter thickness and emitter doping is depicted in Fig. 6. Here, the base doping and thickness are fixed to experimental values (N_A=3x10^{17}/cm^3; 2 μm) to create this contour plot. The carrier mobility was assumed to be constant with the variation of doping concentration. The fill factor is corrected to include the increased series resistance and reduced fill factor associated with low doping levels. As can be seen from the plot, when N_D=3x10^{14}/cm^3 and emitter thickness is 0.6 μm, the cell efficiency reaches 5.16%, which is higher than measured 3.13%. These results differ from previous work because of challenges in achieving the required doping profile in experiments. Although it may be difficult to fabricate lightly-doped doped layers with typical methods, improvements in both V_{oc} and J_{sc} have been identified with reduced emitter doping in the literature [19, 20].

As an alternative method for improving cell efficiency, we may consider adding an intrinsic GaInP layer between the emitter and base layer to form an n-i-p structure [21]. Despite the fact that there is a strong electric field at the depletion region of the modeled cell, the depletion width is only 30 nm. Adding an intrinsic layer could greatly expand the space charge region to improve the collection of carriers excited by the absorbed photons. It is expected that the carrier collection efficiency and J_{sc} will both be improved with higher quantum efficiency over the effective wavelength range after adding the intrinsic layer. With emitter doping and thickness fixed at the

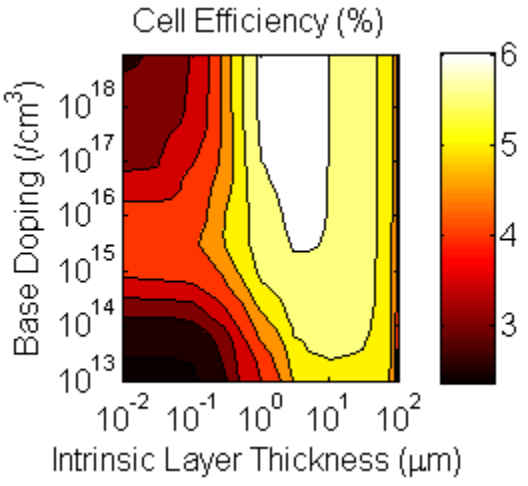

Fig. 7. A contour plot optimizing the cell efficiency as a function of the intrinsic layer thickness and base doping. The highest efficiency of 6.3% is for N_A=9×10^{17}/cm^3 and t_i=2 μm.

experimental values (N_D=1x10^{18}/cm^3; 0.1 μm), cell efficiency as a function of intrinsic layer thickness and base doping is plotted and illustrated in Fig 7.

The cell efficiency is more sensitive to the intrinsic layer thickness than the base doping, within the region considered. With base doping constrained to be smaller than emitter doping, the highest efficiency of 6.3% is obtained at N_A=9×10^{17}/cm^3 and the intrinsic layer thickness t_i of 2 μm, well above the original 3.13%. Efficiency was doubled by greatly extending the space charge region to collect a broader range of generated carriers at different wavelengths. Using these results, the typical external quantum efficiency is illustrated and compared to our prior model result shown in Fig 8. As expected

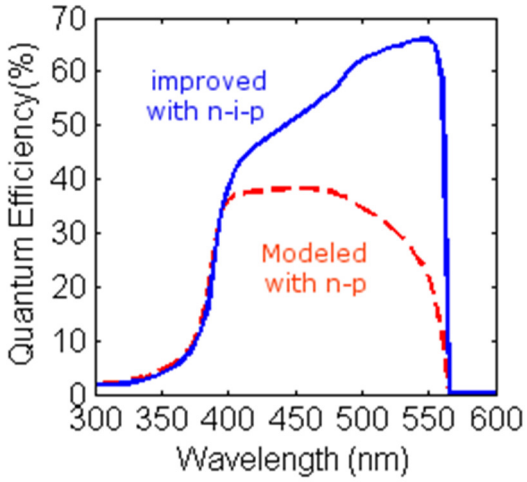

Fig. 8. EQE versus wavelength from 300 nm to 600 nm before and after optimization. Modeled data (dashed red line) is the best fit curve from measured EQE (Ref. 12). The EQE of proposed n-i-p structure with intrinsic layer thickness of 2 μm accounts for all the loss mechanisms found in experiment (blue line).

the quantum efficiency of photons with energies near the band edge increases significantly from the previous design. If this structure (shown in Fig. 9) were to be employed, the new J_{sc} would be 5.44 mA/cm^2, a 70 % improvement over the previous design without requiring any fundamental changes in the growth process. Ion implantation may be employed to sandwich an intrinsic layer between two heavily doped layers in experiment.

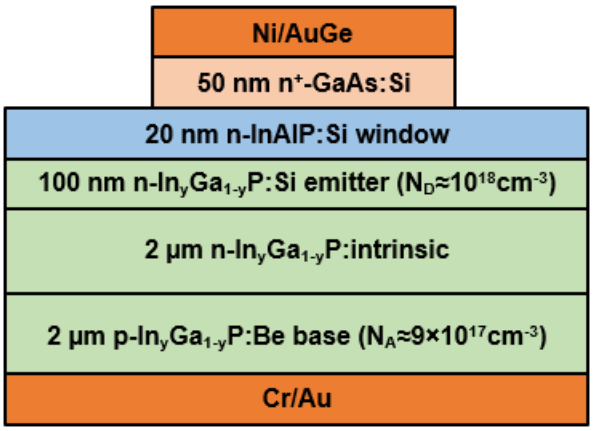

Fig. 9. Cross-sectional schematic of the improved $Ga_{1-y}In_yP$ n-i-p cell structure proposed in this work.

V. Conclusions

In this work, we were able to precisely reproduce the EQE, J_{sc} and V_{oc} associated with a wide bandgap GaInP (E_g = 2.19 eV) photovoltaic cell and found that the emitter and base minority carrier lifetime (τ_e and τ_b) are in the order of 0.1 ns, while the window-emitter interface recombination velocity is approximately $9x10^5$ cm/s. A potential improvement to the cell structure, consisting of adding an intrinsic layer within the junction to form an n-i-p structure is proposed. With intrinsic layer thickness of 2 µm, and base doping of 9×10^{17} /cm^3, this n-i-p single junction wide-E_g GaInP solar cell could achieve an efficiency of 6.3%, a 2× improvement over the n-p design. In future work, we will consider a broader range of GaInP compositions and some intermediate milestones for reduced recombination, as well as their projected benefits. This will help define a path forward to improve the performance much closer to its theoretical limits (approximately 16.5%) [22].

Acknowledgments

Support was provided by the Department of Energy, under DOE Cooperative Agreement No. DE-EE0004946 (PVMI Bay Area PV Consortium), the Semiconductor Research Corporation, under Research Task No. 2110.006 (Network for Photovoltaic Technologies), and the National Science Foundation Award EEC1454315-CAREER: Thermophotonics for Efficient Harvesting of Waste Heat as Electricity.

References

[1] W. Shockley and H. J. Queisser, "Detailed Balance Limit of Efficiency of p-n Junction Solar Cells," *Journal of Applied Physics*, vol. 32, pp. 510–519, 1961.

[2] V. Ganapati, C.-S. Ho, and E. Yablonovitch, "Air Gaps as Intermediate Selective Reflectors to Reach Theoretical Efficiency Limits of Multibandgap Solar Cells," *IEEE Journal of Photovoltaics*, vol. 5(1), pp. 410–417, Jan. 2015.

[3] E. D. Kosten, E. C. Warmann, J. Lloyd, and H. A. Atwater, "Spectrum splitting photovoltaics: light trapping filtered concentrator for ultrahigh photovoltaic efficiency," in *SPIE Proceedings*, 2013, vol. 8821, p. 882109.

[4] J. J. Wysocki and P. Rappaport, "Effect of Temperature on Photovoltaic Solar Energy Conversion," *Journal of Applied Physics*, vol. 31(3), pp. 571–578, Mar. 1960.

[5] K. H. Montgomery, C. Heredia, and J. M. Woodall, "Design and modeling of a high efficiency hybrid photovoltaic-photothermal concentrator (PVPTC) system," in *Photovoltaic Specialists Conference (PVSC), 2013 IEEE 39th*, 2013, pp. 1755–1760.

[6] P. P. Jenkins, S. Messenger, K. M. Trautz, S. I. Maximenko, D. Goldstein, D. Scheiman, R. Hoheisel, and R. J. Walters, "High-Bandgap Solar Cells for Underwater Photovoltaic Applications," *IEEE Journal of Photovoltaics*, vol. 4(1), pp. 202–207, 2014.

[7] S. Wojtczuk, P. Chiu, X. Zhang, D. Pulver, C. Harris, and M. Timmons, "Bifacial Growth InGaP/GaAs/InGaAs Concentrator Solar Cells," *IEEE Journal of Photovoltaics*, vol. 2(3), pp. 371-376, 2012.

[8] F. A. Kish, F. M. Steranka, D. C. DeFevere, D. A. Vanderwater, K. G. Park, C. P. Kuo, T. D. Osentowski, M. J. Peanasky, J. G. Yu, R. M. Fletcher, D. A. Steigerwald, M. G. Craford, V. M. Robbins, "Very high-efficiency semiconductor wafer-bonded transparent-substrate $(Al_xGa_{1-x})_{0.5}Ga_{0.5}P$/GaP light emitting diodes," *Applied Physics Letters*, vol. 64(21), pp.2839-2841, 1994.

[9] M. Yamaguchi, T. Takamoto, K. Araki, and N. Ekins-Daukes, "Multi-junction III–V solar cells: current status and future potential," *Solar Energy*, vol. 79(1), pp. 78-85, 2005.

[10] R. R. King, D. Bhusari, A. Boca, D. Larrabee, X. Q. Liu, W. Hong, C. M. Fetzer, D. C. Law and N. H. Karam, "Bandgap-voltage offset and energy production in next-generation multijunction solar cells," *Progress in Photovoltaics: Research and Applications*, vol. 19(7), pp. 797-812, 2011.

[11] X. Lu, R. Hao, M. Diaz, R. L. Opila, and A. Barnett, "Improving GaP Solar Cell Performance by Passivating the Surface Using $Al_xGa_{1-x}P$ Epi-Layer," *Electron Devices Society, IEEE Journal of the*, vol. 1(5), pp. 111–116, 2013.

[12] S. Tomasulo, J. Faucher, J. R. Lang, K. N. Yaung, and M. L. Lee, "2.19 eV InGaP solar cells on GaP substrates," in *Photovoltaic Specialists Conference (PVSC), 2013 IEEE 39th*, 2013, pp. 3324–3328; S. Tomasulo, K.N. Yaung, J. Faucher, M. Vaisman, and M. L. Lee. "Metamorphic 2.1-2.2 eV InGaP solar cells on GaP substrates." *Applied Physics Letters*, 104(17), p. 173903, 2014.

[13] Bermel, P., M. Ghebrebrhan, W. Chan, Y. X. Yeng, M. Araghchini, R. Hamam, … and I. Celanovic. (2010). "Design and global optimization of high-efficiency thermophotovoltaic systems." *Optics express*, *18*(103), A314-A334.

[14] J. Gray, X. Wang, R. Chavali, X. Sun, A. Kanti, J. R. Wilcox (2011), "ADEPT 2.1," https://nanohub.org/resources/adeptnpt.

[15] Schubert, E. Fred, Thomas Gessmann, and Jong Kyu Kim. *Light emitting diodes*. John Wiley & Sons, Inc., 2005.

[16] Park, K. W., C. Y. Park, S. Ravindran, S. J. Kang, H. Y. Hwang, Y. D. Jho, Y. R. Jo, B. J. Kim, and Y. T. Lee. "Enhancement of minority carrier lifetime of GaInP with lateral composition modulation structure grown by molecular beam epitaxy." *Journal of Applied Physics*, 116(4), p. 043516, 2014.

[17] Allen, C. R., J. M. Woodall, and J-H. Jeon. "Results of a photovoltaic junction with an AR coating under concentration of natural sunlight." *Solar Energy Material and Solar Cells*, 95(9), pp. 2655-2658, 2011.

[18] Vaisman, M., S. Tomasulo, T. Masuda, J. R. Lang, J. Faucher, and M. L. Lee “Effects of growth temperature and device structure on GaP solar cells grown by molecular beam epitaxy.” *Applied Physics Letters*, 106(6), p.063903, 2015.

[19] Blakers, A. W., and M. A. Green. "20% efficiency silicon solar cells." *Applied physics letters* 48(3), pp. 215-217, 1986.

[20] Wanlass, M. W., G. S. Horner, T. A. Gessert, T. J. Coutts, and I. Weinberg. "Epitaxial InP And Related III-V Compounds Applied To SolarCells." In 1st Intl Conf on Idium Phosphide and Related Materials for Advanced Electronic and Optical Devices, pp.445-458. *International Society for Optics and Photonics*, 1989.

[21] Cheah, W. K., W. J. Fan, S. F. Yoon, D. H. Zhang, B. K. Ng, W. K. Loke, R. Liu, and A. T. S. Wee. "GaAs-based heterojunction pin photodetectors using pentanary InGaAsNSb as the intrinsic layer." *Photonics Technology Letters*, *IEEE* 17(9), pp. 1932-1934. 2005

[22] Shalav, A., B. S. Richards, and M. A. Green. "Luminescent layers for enhanced silicon solar cell performance: Up-conversion." *Solar Energy Materials and Solar Cells* 91(9), pp. 829-842, 2007